applied sciences

MDPI

Article

Mechanical Manipulation of Diffractive Properties of Optical Holographic Gratings from Liquid Crystalline Elastomers

Dejan Bošnjaković [1,2], Marko Gregorc [1], Hui Li [3,4], Martin Čopič [1,5], Valentina Domenici [6] and Irena Drevenšek-Olenik [1,5,*]

1 Faculty of Mathematics and Physics, University of Ljubljana, Jadranska 19, 1000 Ljubljana, Slovenia; dejan.bosnjakovic@ferit.hr (D.B.); mark.gregorc@gmail.com (M.G.); martin.copic@fmf.uni-lj.si (M.Č.)
2 Faculty of Electrical Engineering, Computer Science and Information Technology, Josip Juraj Strossmayer University of Osijek, Kneza Trpimira 2B, 31000 Osijek, Croatia
3 Tianjin Economic-Technology Development Area Institute of Applied Physics & School of Physics, Nankai University, Tianjin 300071, China; hli@lps.ecnu.edu.cn
4 State Key Laboratory of Precision Spectroscopy, East China Normal University, Shanghai 200062, China
5 J. Stefan Institute, Jamova 39, SI 1001 Ljubljana, Slovenia
6 Dipartimento di Chimica e Chimica Industriale, Università degli studi di Pisa, via Moruzzi 13, 56126 Pisa, Italy; valentina.domenici@unipi.it
* Correspondence: irena.drevensek@ijs.si; Tel.: +386-1-4773-647

Received: 3 July 2018; Accepted: 4 August 2018; Published: 9 August 2018

Abstract: An appealing property of optical diffractive structures from elastomeric materials is a possibility to regulate their optical patterns and consequently also their diffractive features with mechanical straining. We investigated the effect of strain on diffraction characteristics of holographic gratings recorded in a monodomain side-chain liquid crystalline elastomer. The strain was imposed either parallel or perpendicular to the initial alignment direction of the material. At temperatures far below the nematic–paranematic phase transition, straining along the initial alignment affects mainly the diffraction pattern, while the diffraction efficiency remains almost constant. In contrast, at temperatures close to the nematic–paranematic phase transition, the diffraction efficiency is also significantly affected. Straining in the direction perpendicular to the initial alignment strongly and diversely influences both the diffraction pattern and the diffraction efficiency. The difference between the two cases is attributed to shear–stripe domains, which form only during straining perpendicular to the initial alignment and cause optical diffraction that competes with the diffraction from the holographic grating structure.

Keywords: liquid crystalline elastomers; holographic gratings; optical diffraction; elasto-optic effect

1. Introduction

Light-sensitive liquid crystalline elastomers (LS-LCEs) are soft materials that combine an orientational order of liquid crystals and the rubber elasticity of elastomers with the photoresponsivity of photoisomerizable compounds [1–3]. As optical holographic materials, they show many intriguing properties. For instance, they exhibit recording sensitivity that is several orders of magnitude larger than conventional (non-liquid crystalline) elastomers containing similar photoisomerizable moieties [4–9]. The recording process takes place in a very nonlinear manner that allows an intricate control over the spatial structuring of the refractive index modulation. The associated diffraction effects are particularly interesting in the temperature region close to the nematic–paranematic phase transition, in which phenomena such as the recording of "hidden holograms" and "hologram dark

enhancement effect" can be observed [10]. Light-sensitive LCEs are also very efficient for recording polarization gratings generated by the superposition of orthogonally polarized writing beams. In the vicinity of the Bragg angle, those gratings exhibit an unusual splitting of the diffraction peak, which is a consequence of the strong absorption anisotropy for the actinic optical radiation [11].

All of the above-mentioned properties are predominantly associated with the liquid crystalline character of the LCEs. However, their elastomeric character can also yield several interesting features. The most evident one is the possibility of regulating the spatial periodicity of optical patterns by mechanical straining, which was demonstrated in our recent study, and which makes LCE films very promising for applications in mechanically tunable diffractive optical elements, such as adjustable optical filters or stretchable diffractive lenses [12]. However, in designing practical devices, it is very important to know not only how mechanical manipulation affects the diffracted patterns, but also how it affects the efficiency of the related diffractive phenomena. Consequently, in this work, the emphasis is on the effects of stress and strain on the diffraction efficiency of some selected holographic grating structures.

The stress–strain relationship $\sigma(\varepsilon)$ of an orientationally aligned (monodomain) LCE film strongly depends on the straining direction. For straining along the preferential orientation of the liquid crystalline (mesogenic) molecular units, known as the nematic director $\mathbf{n_0}$, stress increases proportionally to strain, similar to conventional elastomers. For straining in the direction perpendicular to $\mathbf{n_0}$, a nonlinear behavior known as (semi)soft elasticity is observed, which is characterized by a plateau region in which stress remains nearly constant during the increasing strain [1,13]. This phenomenon is associated with a continuous reorientation of the mesogenic molecular units in the embedding polymer network. The exact dependence of $\sigma(\varepsilon)$ is affected also by the sample preparation procedure and by the temperature. For LCE materials with a smooth (continuous) phase transition from the nematic to the isotropic phase (also called paranematic phase) [14,15], as the one used in our study, the behavior of $\sigma(\varepsilon)$ is also smooth at all temperatures. The anisotropy of the stress–strain relationship decreases with the increasing temperature, and more or less vanishes at the transition temperature T_0 [16,17]. In LS-LCEs, illumination with ultraviolet (UV) light affects the stress–strain relationship in a similar manner as heating, i.e., it causes a decrease of the liquid crystalline order that is governed by the illumination intensity [2,18–20]. The experiments exploring this effect are usually performed either with homogeneous or with macropatterned UV illumination generated with the use of photolithographic masks [4,13,21–23], while in our study, we used micropatterned UV illumination generated by holographic lithography.

2. Experimental

Macroscopically aligned (single domain) polysiloxane-based LS-LCE films were prepared by the two-step "Finkelmann cross-linking procedure" [24]. The cross-linker concentration was 5 wt% and the photosensitive azomesogen concentration was 9 wt%. The azomesogens and also the conventional mesogens were attached to the polysiloxane backbone as side groups. The details of the synthesis method and sample preparation procedures are described elsewhere [6]. The thickness of the films was 150 μm. Samples of rectangular shape with a typical surface area of around 5×5 mm^2 were cut out from the films. For probing strain-induced modifications of diffractive properties, one edge of the sample was clamped to the frame of the sample holder, while the other edge was attached to the translation stage used for imposing a controlled tensile strain (see Figure 1). The straining was performed either along or perpendicular to the initial alignment direction $\mathbf{n_0}$. For probing illumination-induced stress modifications, the sample was slightly prestrained, and then clamped to the strain gauge that was used to measure the tensile force. The force was measured via two resistive type sensors, in which resistance is very sensitive to contraction/expansion. They were attached to the frame of the sample holder, as indicated in Figure 1b.

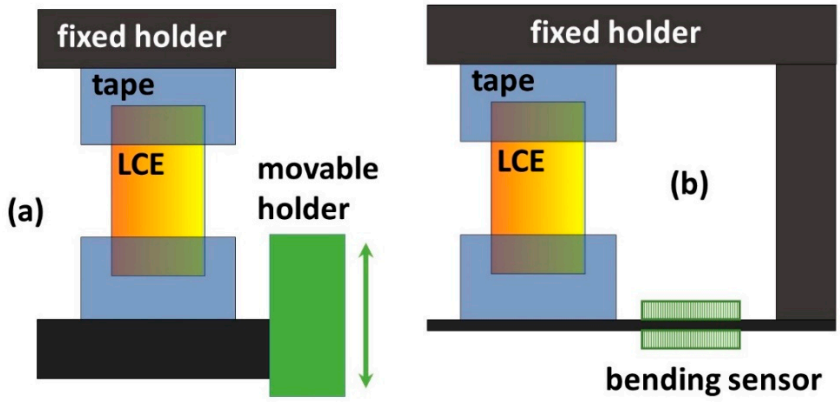

Figure 1. Schematic drawing of the sample mount used for (**a**) investigations of the effects of stretching and (**b**) investigations with a fixed sample length. Yellow rectangle denotes the liquid crystalline elastomers (LCE) film, blue denotes the adhesive tape (Capton tape), and black denotes the metallic holders. The green rectangle in (**a**) denotes the end part of a translation stage, and the green rectangles in (**b**) denote resistive sensors used to detect the small bending of the lower part of the holder. The corresponding (calibrated) variations of the resistivity provide information on the tensile force in the sample. The entire setup was build up on the standard optical table (mechanical vibration isolation platform).

The investigated one-dimensional and two-dimensional holographic transmission gratings were recorded either with two or four intersecting UV laser beams from an argon ion laser operating at the recording wavelength of λ_R = 351 nm. All of the beams were expanded to the area with a diameter d_R ~ 10 mm, which was considerably larger than the LCE film, and were linearly polarized in the direction parallel to $\mathbf{n_0}$ (extraordinary polarization). The average power density of UV radiation on the sample during the recording process was ~20 mW/cm^2, and the typical illumination time was several minutes. In the two-beam configuration, the intensity pattern is described as [7]:

$$I(x) = I_0(\cos(k_\perp x))^2, \tag{1}$$

where $k_\perp = k_0 \sin\alpha$ is the transversal component of the wave vector of incident beams, α is the incidence angle (with respect to surface normal), and k_0 is the wave vector in vacuum. This pattern induces a one-dimensional modulation of the optical properties of the sample with a periodicity of $\Lambda = \pi/k_\perp$ along the x axis. In the four-beam configuration, the intensity pattern is given as [25]:

$$I(x,y) = \mathrm{I}_0(\cos(k_\perp x) + \cos(k_\perp y))^2, \tag{2}$$

which corresponds to the quadratic lattice oriented at 45° with respect to the x and y axes. The lattice distance (unit cell dimension) is $a = \sqrt{2}\pi/k_\perp$ and the diagonal of the unit cell is $D = 2\pi/k_\perp$.

The diffraction properties of the recorded grating structures were probed with a low-power beam (<1 mW) from a HeNe laser operating at a probing wavelength of λ_P = 633 nm. As this wavelength is far from the absorption peaks of the material, it is affected mainly by the phase-type modulation of optical properties [26]. The probe beam was linearly polarized in the direction of extraordinary polarization, and entered the film at normal incidence. The spot size of the probe beam in the film was d_p ~0.2 mm, which is much smaller than the diameter of the recording beams [27]. The far field diffraction pattern was detected either with a CCD camera (strain-induced effects) or by a set of photodiodes (experiments with fixed sample length) placed at the distance of 0.5 m behind the sample.

3. Results

The dominant origin of holographic recording in LS-LCEs is UV illumination-induced *trans*-to-*cis* isomerization of azomesogenic side groups [5,28,29]. The rate of this process is proportional to the intensity of the UV irradiation; therefore, it predominantly takes place in the regions of high intensity, while in the regions of low intensity, it is nearly absent. Consequently, a spatially modulated concentration of the *cis* isomers $N_c(\mathbf{r})$ is established. *Cis* isomers act as impurities in the liquid crystalline phase [18], so they cause a local decrease of the scalar nematic order parameter S ($S =< (3\cos^2\theta - 1)/2 >$), where θ is the angle between the long axis of the mesogenic molecules and the direction $\mathbf{n_0}$, and brackets denote averaging), which can be described as:

$$S(\boldsymbol{r}, T) = S_0(T) + \Delta S(N_c(\boldsymbol{r}), T), \tag{3}$$

where S_0 corresponds to the order parameter in the dark (when all of the azomesogens are in the *trans* state), $\Delta S < 0$ is the isomerization-induced modification of S, $N_c(\mathbf{r})$ the concentration of *cis* azomesogens at a selected position $\mathbf{r}$, and T is the temperature.

Local modifications of S result in modifications of optical birefringence of the material $n_b = (n_e - n_o) \propto S$, where e and o denote the extraordinary and the ordinary ray, respectively. Therefore, after illumination with the periodic UV interference pattern, n_o as well as n_e become periodically modulated, i.e., an anisotropic optical grating structure is formed [9]. This structure decays with time due to spontaneous *cis*-to-*trans* back isomerization of the azomesogens. The decay process is exponential, and the corresponding decay time τ, as a function of the temperature, exhibits the Arrhenius behavior [30]. For the investigated LCE material, the value of τ at room temperature (23 °C) is around 250 min, while at transition temperature T_0 = 81.6 °C, it decreases to about 5 min. The spontaneous decay of the grating structure is of course not suitable for practical applications, but it is very convenient for research purposes, because the one and same sample can be used to perform different experiments. The decay of recorded patterns can be prevented by using photosensitive mesogens with very long lifetimes of the *cis* isomer, or by using the light-induced covalent attachment of mesogenic groups to the polymer backbone [31,32].

In the experiments performed at room temperature, we first recorded the grating, and then analyzed its diffraction properties as a function of strain. The length of the sample was increased or decreased in steps of few micrometers, corresponding to strain in the interval from 0 to a maximum of 15%. The time interval between subsequent measurements was 1 min, which provided enough time for the equilibration of the structure. Figure 2a shows the observed dependence of a relative elongation of the lattice period of a one-dimensional grating (line grating) with Λ = 2.3 μm as a function of the tensile strain $\varepsilon_{\|}$ applied in the direction parallel to $\mathbf{n_0}$. For modulation along $\mathbf{n_0}$, the value of $\Delta\Lambda/\Lambda$ increases with increasing strain, while for modulation perpendicular to $\mathbf{n_0}$, it decreases with increasing strain. The decrease observed in the latter case is about two times smaller than the increase observed in the former case, which is in agreement with the volume conservation of the material [1]. The values of $\Delta\Lambda/\Lambda$ obtained during increasing (solid symbols) and decreasing strain (open symbols) are very similar, i.e., the behavior is reversible. Figure 2b shows the results of an analogous experiment performed with a two-dimensional grating with unit cell dimensions a = 13.5 μm and D = 19.1 μm. Due to stretching, the square lattice is transformed to a diamond (rhomboidal) lattice with different unit cell diagonals D_L and D_T in directions parallel and perpendicular to $\mathbf{n_0}$, respectively (see insert). The observed relative modifications $\Delta D_\mathrm{L}/\mathrm{D}$ and $\Delta D_\mathrm{T}/\mathrm{D}$ as a function of $\varepsilon_{\|}$ are very similar to those obtained for one-dimensional gratings.

Figure 3 shows the relative intensity of diffraction peaks $I_\mathrm{d}/I_\mathrm{d0}$ as a function of $\varepsilon_{\|}$, where I_d0 denotes diffracted intensity at $\varepsilon_{\|}$ = 0. The peaks associated with diffraction from diagonal lattice planes separated for $D_\mathrm{L}/2$ (denoted in the insert as peaks 11 and $\overline{11}$) and $D_\mathrm{T}/2$ (peaks $\bar{1}1$ and $1\bar{1}$) were analyzed. For longitudinal (L) peaks, the intensity is practically constant, while for transversal (T) peaks, it slightly decreases with increasing strain. At this point, it should be mentioned that the data

shown in Figure 3 are already renormalized for the decrease of intensity associated with the *cis*-to-*trans* back isomerization, i.e., the original measured intensity is multiplied with the factor $e^{(t/\tau)}$, where τ is the *cis*-to-*trans* back-relaxation time measured at $\varepsilon_{||} = 0$, and t is the time passed since switching off the recording beams [30], so they solely reveal the effects associated with strain.

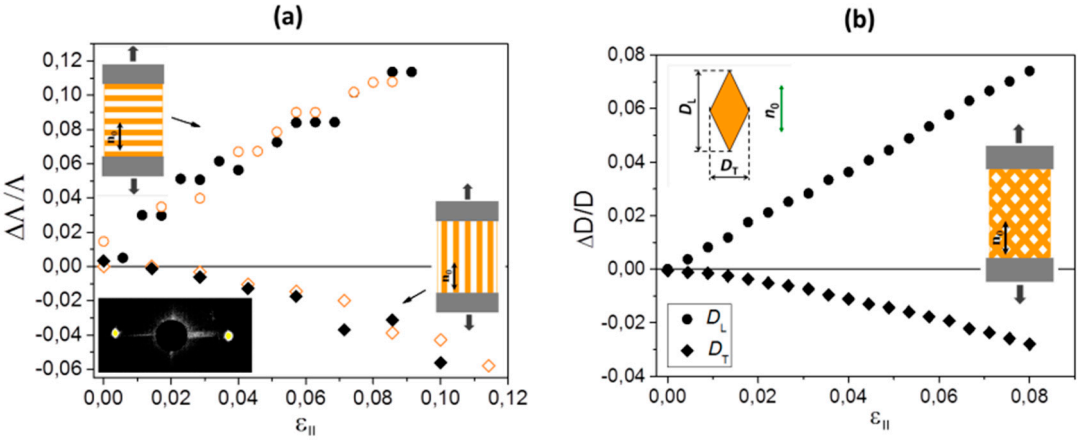

Figure 2. (**a**) Relative modification of grating periodicity Λ of a one-dimensional grating as a function of tensile strain $\varepsilon_{||}$ applied parallel to the alignment direction $\mathbf{n_0}$. Solid symbols correspond to increasing strain and open symbols to decreasing strain. The drawings illustrate the orientation of the grating lines with respect to $\mathbf{n_0}$. The arrows indicate the direction of strain. The insert in the lower left corner shows the far field diffraction pattern observed on a screen. The transmitted beam was blocked, so that only the first-order diffraction peaks can be seen. (**b**) Relative modification of unit cell diagonals D of a two-dimensional square grating as a function of $\varepsilon_{||}$. The drawing on the left side shows a rhomboidal unit cell with the longitudinal diagonal D_L and the transversal diagonal D_T. The drawing on the right side shows the orientation of the 2D lattice with respect to $\mathbf{n_0}$.

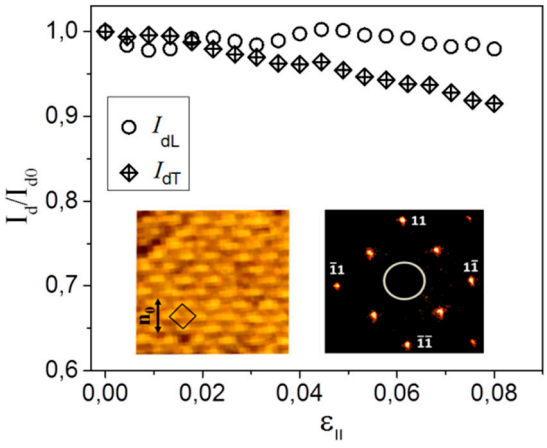

Figure 3. Relative modification of intensity I_d of optical diffraction peaks from a two-dimensional square grating as a function of the tensile strain $\varepsilon_{||}$ applied in the direction parallel to the alignment direction $\mathbf{n_0}$. The insert on the left shows the polarization optical microscopy (POM) image of the sample with a superimposed unit cell. The insert on the right shows the far field diffraction pattern observed on a white screen. The transmitted beam is blocked. The diffraction peaks 11 and $\overline{11}$ (longitudinal (L) peaks) and $\bar{1}1$ and $1\bar{1}$ (transversal (T) peaks) are marked.

If the film is strained in the direction perpendicular to $\mathbf{n_0}$, strain-induced modifications of the grating periodicity show similar behavior as observed for straining along $\mathbf{n_0}$. Figure 4 shows the

dependence of a relative elongation of the period of a one-dimensional grating with Λ = 2.5 μm as a function of the tensile strain $\varepsilon_\perp$ applied in the direction perpendicular to $\mathbf{n_0}$. Also in this case, for modulation along $\mathbf{n_0}$, the value of $\Delta\Lambda/\Lambda$ increases with increasing strain, while for modulation perpendicular to $\mathbf{n_0}$, it decreases with increasing strain. However, a decrease observed in the latter case has nearly the same magnitude as the increase observed in the former case, which signifies an asymmetry in the transversal shrinking process. Further studies of grating structures with different values of Λ are needed to resolve the details of this interesting process. The values obtained during increasing (solid symbols) and decreasing strain (open symbols) are quite similar, but they exhibit some hysteresis.

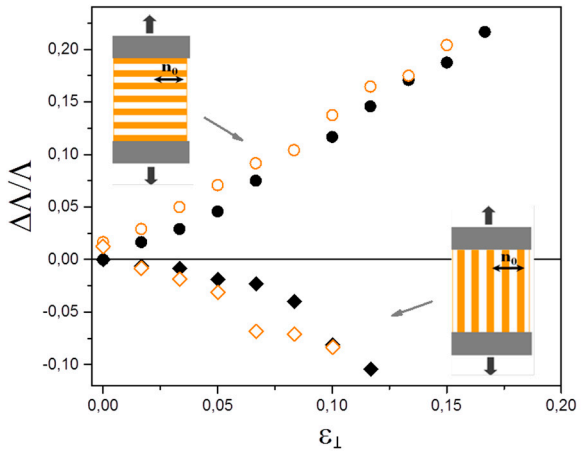

Figure 4. Relative modification of grating periodicity Λ of a one-dimensional line grating as a function of the tensile strain $\varepsilon_\perp$ applied in the direction perpendicular to the alignment direction $\mathbf{n_0}$. Solid symbols correspond to the increasing strain, and open symbols correspond to the decreasing strain. The drawings illustrate orientation of the grating lines with respect to $\mathbf{n_0}$. The arrows indicate the direction of strain.

The hysteresis is even more evident in the dependence of the diffracted intensity I_d of the first-order diffraction peaks on $\varepsilon_\perp$ shown in Figure 5a. The diffracted intensity observed after a full cycle of stretching and contraction of the sample is also about 10% lower than in the beginning. However, the most evident observation of this experiment is that the value of I_d/I_{d0} strongly decreases with increasing strain, and drops for about a factor of five during straining from $\varepsilon_\perp = 0$ to $\varepsilon_\perp = 0{,}17$. Another interesting observation is that with increasing strain, the form of the diffraction peaks is transformed from a nearly circular spot to an elongated cloud. This is attributed to the formation of shear–stripe domains that accompany the reorientation process of the director field [33,34]. The stripes are oriented perpendicular to $\mathbf{n_0}$, and typically have a thickness of around 10 μm. Consequently, they cause strong light scattering in the direction parallel to $\mathbf{n_0}$ (see insets in Figure 5a), and therefore, the outgoing peaks become elongated. In determination of the diffraction efficiency, this effect was taken into account by integrating the diffracted intensity in the elongated regions marked as rectangles in the inset of Figure 5a.

The results obtained for the grating with grating lines parallel to $\mathbf{n_0}$ are shown in Figure 5b. In this case, the two effects mentioned above are superimposed on each other (see inset of Figure 5b) and for $\varepsilon_\perp \geq 0.12$, it is practically impossible to separate the diffraction from holographic grating from the diffraction from the strain-induced striped structure. For that reason, the measurements of I_d/I_{d0} as a function of $\varepsilon_\perp$ were limited to $\varepsilon_\perp < 0.12$. A profound hysteresis is observed during the stretching–contraction cycle. Besides this, opposite to the situation in Figure 5a, the value of I_d/I_{d0} strongly increases with increasing strain. The increase for a factor of 10 is obtained for straining

from $\varepsilon_\perp = 0$ to $\varepsilon_\perp = 0.12$. Also in this case, the data shown are already renormalized for the decrease associated with the *cis*-to-*trans* back-isomerization.

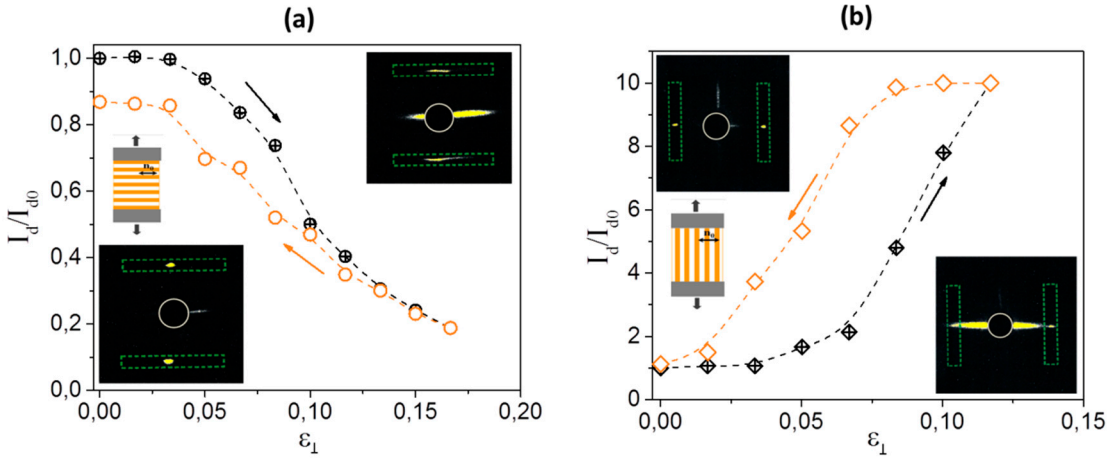

Figure 5. (**a**) Relative modification of intensity of first-order diffraction peaks I_d for a one-dimensional grating with grating lines parallel to $\mathbf{n_0}$. The insert in the lower left corner shows the far-field diffraction pattern observed at $\varepsilon_\perp = 0$. The transmitted beam was blocked, so that only the first-order diffraction peaks can be seen. The insert in the upper right corner shows the far-field diffraction pattern observed at $\varepsilon_\perp = 0.1$. Elongation of diffraction peaks due to light scattering from striped domains can be noticed. Squares denote the regions of integration that are used to determine the intensity of the diffraction peaks. (**b**) Relative modification of I_d for a one-dimensional grating structure with grating lines perpendicular to $\mathbf{n_0}$. The inserts in the upper left and lower right corners show far field diffraction patterns at $\varepsilon_\perp = 0$ and $\varepsilon_\perp = 0.1$, respectively. The elongation of diffraction peaks due to light scattering from striped domains can again be noticed. Squares denote regions of integration that have been used to determine the intensity of diffraction peaks.

For a square holographic grating with the lattice distance a = 13.5 μm, the scattering from stripe domains smears out the diffraction from the grating structure already for $\varepsilon_\perp \geq 0.03$, which prevents reasonable measurements of the strain-induced effects on the holographic pattern. Consequently, this grating structure was not investigated in the configuration in which the strain is applied perpendicular to $\mathbf{n_0}$. For a specific measurement in the selected sample region, the uncertainty of the experimental data shown in Figures 2–5 is within the size of the data points. However, when measurements are performed in different sample regions, the variations might be larger, as some imperfections and inhomogeneities are usually present within the sample structure.

At temperatures in the vicinity of T_0 (81.6 °C), the *cis*-to-*trans* back-isomerization of the azomesogens is so fast that systematic measurements of the effect of strain on diffraction properties, as described above, are not possible. Hence, at these temperatures we used another setup, in which the sample was clamped to the frame with two sides and consequently had a fixed length, and we performed in situ monitoring of the tensile force and diffraction intensity during recording and relaxation of the holographic patterns. Before clamping, the sample was slightly prestrained. Also in this case, the measurements were performed in two configurations: for clamping along $\mathbf{n_0}$ and for clamping perpendicular to $\mathbf{n_0}$.

Figure 6 shows the results obtained for clamping along $\mathbf{n_0}$ at T = 75 °C. One-dimensional UV interference pattern with Λ = 9.5 μm was recorded. Figure 6a shows relative modifications of the force $\Delta F/F_0$ as a function of time obtained for three different prestraining forces F_0 applied to the film. The value F_0 = 1 mN corresponds to the tensile stress of σ ~2 kPa. The exact value of σ is difficult to be determined, because clamping affects the cross-section of the film. The tensile force F increases during the recording process (0 < t < 5 min), while after switching off the UV light, it decreases back to the

initial value. The relaxation process is monotonic, and takes place in two stages: a fast one on a time scale of seconds, which is attributed to thermal effects, and a slower one on a time scale of minutes, which is attributed to *cis*-to-*trans* back isomerization.

Figure 6b shows the temporal dependence of diffracted intensity I_d of the probe beam. Despite the sample being clamped at two opposite edges and hence being unable to be shrunk due to UV illumination, the value of I_d strongly fluctuates during the recording process. The fluctuations differ from one recording process to another, and are in general larger at larger clamping forces. They are attributed to inhomogeneous modifications of the material structure during the illumination. Regions of film that are slightly softer than the surrounding expand on behalf of the harder regions. If the structure is fully homogeneous, contraction cannot happen due to clamping. However, if some parts of the sample are softer than others, the softer parts can extend so that the harder ones can shrink, but the entire sample length remains the same. Consequently, the recording medium moves with respect to the interference pattern. The effect is similar to the fluctuations caused by vibrations in the optical setup [35]. The two effects are difficult to be resolved from each other. Consequently, it is difficult to compare the values of diffracted intensity observed at the end of subsequent recording processes with each other; therefore, we show absolute instead of relative results. However, after the UV beams are switched off, the behavior observed for all three cases is very similar, and exhibits an increase of diffraction intensity known as "dark hologram enhancement effect". This effect is associated with a strongly nonlinear relationship between the concentration of the *cis* azo-mesogens N_c and the nematic order parameter S that is characteristic for temperatures in the vicinity of T_0, which was extensively discussed in our previous work [10]. The present study reveals that the enhancement significantly increases with the increasing prestraining force F_0.

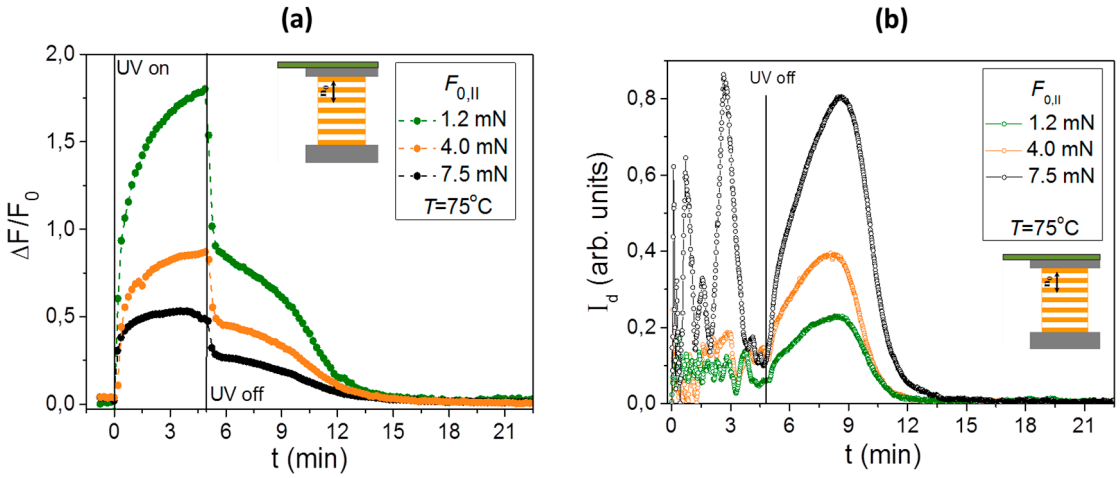

Figure 6. (**a**) Time dependence of a relative modification of tensile force F during the recording and relaxation processes. The sample was clamped in the direction parallel to $\mathbf{n_0}$. The drawing illustrates the orientation of the sample with respect to the grating lines. The inset gives the values of the prestraining force F_0. (**b**) Time dependence of intensity of optical diffraction peaks I_d during the recording and relaxation processes.

The results of an analogous experiment with straining in the direction perpendicular to $\mathbf{n_0}$ are shown in Figure 7. The observed features are very similar to those obtained for straining along $\mathbf{n_0}$. Only the sign of the force modifications $\Delta F/F_0$ is opposite, which means that the tensile force decreases during UV illumination. The graphs for $\Delta F/F_0$ and I_d as a function of time are plotted together. Figure 7a shows the results obtained for a recording time of 3 min, and Figure 7b shows the results for a recording time of 15 min. Modifications of $\Delta F/F_0$ saturate at $\Delta F/F_0 \sim -0.8$, which corresponds to the net tensile force $F = 0.2\ F_0$ being present in the sample after a prolonged UV illumination. After switching off the UV beams, a two-stage relaxation process takes place again. The effect of

dark hologram enhancement is slightly smaller than for clamping in the direction parallel to $\mathbf{n_0}$, but otherwise, the observed behavior of $I_d(t)$ is very similar and exhibits similar characteristic times.

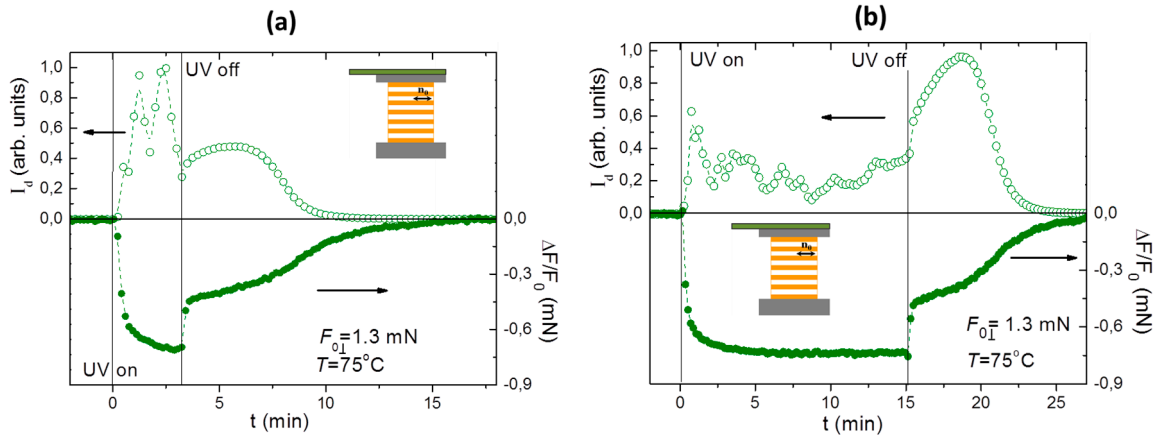

Figure 7. (**a**) Time dependences of I_d and $\Delta F/F_0$ measured during recording and relaxation processes for a recording time of 3 min. The sample was clamped in the direction perpendicular to $\mathbf{n_0}$. The drawing illustrates the orientation of the sample with respect to the grating lines. The inset gives the value of the prestraining force F_0. (**b**) Time dependences of I_d and $\Delta F/F_0$ during the recording and relaxation processes for 15 min of recording.

4. Discussion

In the following, we present a qualitative explanation of the effects of $\varepsilon_{\parallel}$ and $\varepsilon_{\perp}$ on refractive index modulation in a monodomain nematic LCE film. As shown in our recent paper [10], the temperature dependence of the order parameter $S(T)$ and consequently also of the extraordinary refractive index $n_e(T,T_0)$ of such a film can be described by the heuristic function that is in agreement with the Landau theory of supercritical phase transitions [9,36]:

$$n_e(T) = \left[\bar{\varepsilon}_0 + \frac{2}{3}\beta S(T)\right]^{1/2} = \left[\bar{\varepsilon}_0 + A\left\{\left[\left(1 + B|T - T_0|^{\gamma}\right)/B\right]^{1/\gamma} - (T - T_0)\right\}^{1/(\gamma-1)}\right]^{1/2} \quad (4)$$

where $\bar{\varepsilon}_0$ is dielectric permittivity in the paranematic phase ($T >> T_0$), and β is determined by the molecular anisotropy. The values of material parameters γ and B for the investigated material were obtained from the experimental data on the spontaneous elongation of the sample during cooling from the paranematic to the nematic phase, and are $\gamma = 4.8$ and $B = 29$ [10]. The values of the parameters A and $\bar{\varepsilon}_0$ can be deduced from the values of refractive indices of the material at room temperature and at $T >> T_0$. For side-chain LCE materials of the type as the one used in our study, those values are $n_e(T >> T_0) \sim n_o(T >> T_0) = 1.58$, $n_e(T_0 - 50\ °C) = 1.66$, and $n_o(T_0 - 50\ °C) = 1.54$ [37,38], which gives $\bar{\varepsilon}_0 = 2.5$ and $A = 0.077$. The resulting dependence of $n_e(T,T_0)$ is shown as the black solid line in Figure 8a.

The effect of UV illumination-induced *trans*-to-*cis* isomerization on $n_e(T)$ can be modeled as a decrease of the transition temperature $T_0' = T_0 - C_cN_c$, where C_c is a proportionality constant [18]. The corresponding dependence of $n_e(T,T_0')$ for $T_0' = T_0 - 10\ °C$, which is typically realized in the experiments, is shown as the orange solid line in Figure 8a. The vertical difference between the two curves, namely $\Delta n_e(T) = n_e(T,T_0) - n_e(T,T_0')$, corresponds to the refractive index modulation between the dark and the UV-illuminated regions of the unstrained sample.

The effect of $\varepsilon_{\parallel}$ (and of the corresponding stress $\sigma_{\parallel}$), which adds up to the intrinsic strain imposed during the fabrication process, can be modeled as a decrease of the critical exponent $\zeta = 1/(\gamma - 1)$. In addition to this, the value of A needs to be modified due to the strain-induced increase of the order parameter that can be described as $\Delta S = C_{\varepsilon}\varepsilon_{\parallel}$, where C_{ε} is the proportionality constant dependent on the properties of the polymer network [39]. This effect in general results in the increase of n_e with

increasing $\varepsilon_{\|}$ [40]. To illustrate the resulting behavior, the dependences of $n_e(T,T_0,\varepsilon_{\|})$ and $n_e(T,T_0',\varepsilon_{\|})$ corresponding to $\gamma' = 2\gamma = 9.6$ and $A' = 3A = 0.23$ for the unilluminated and for the UV-illuminated strained material are shown as dashed lines in Figure 8a. Also in this case, the vertical difference between the two (dashed) curves $\Delta n_e(T,\varepsilon_{\|}) = n_e(T,T_0,\varepsilon_{\|}) - n_e(T,T_0',\varepsilon_{\|})$ gives the refractive index modulation between the dark and the UV-illuminated regions of the strained sample.

By comparing the vertical separation between the two solid and the two dashed lines, one can notice that at room temperature (23 °C), the modulation of n_e in the strained material is smaller than in the unstrained material, which is in agreement with the experimentally observed decrease of the diffraction efficiency shown in Figure 3. In contrast, at T = 75 °C, the modulation of n_e in the strained material is larger than in the unstrained material, which is in agreement with the results shown in Figure 6b. Therefore, the above described model can well explain the effect of $\varepsilon_{\|}$ on the diffraction efficiency of the grating structures in LS-LCEs.

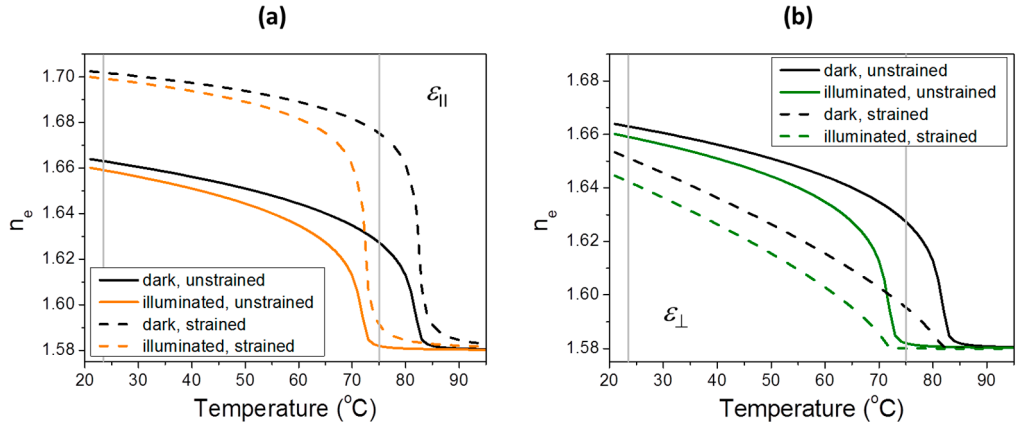

Figure 8. Calculated temperature dependences of extraordinary refractive index n_e of the LCE material based on Equation (4). (**a**) Unstrained and unilluminated (black solid line), unstrained and UV-illuminated (orange solid line), strained along $\mathbf{n_0}$ and unilluminated (black dashed line), and strained along $\mathbf{n_0}$ and UV-illuminated (dashed orange line); (**b**) Unstrained and unilluminated (black solid line), unstrained and UV-illuminated (green solid line), strained perpendicular to $\mathbf{n_0}$ and unilluminated (black dashed line), and strained perpendicular to $\mathbf{n_0}$ and UV-illuminated (dashed green line). Grey vertical lines denote the temperatures at which the experiments were performed.

Straining in the direction perpendicular to $\mathbf{n_0}$ in its initial stage (before reaching the plateau region in the $\sigma(\varepsilon_{\perp})$ curve) causes a decrease of the internal strain, and consequently also a decrease of the order parameter S [39]. This corresponds to the increase of the critical exponent $\zeta = 1/(\gamma - 1)$ and the decrease of the parameter A in Equation (4). To illustrate the associated effects, the dependences of $n_e(T,T_0,\varepsilon_{\perp})$ and $n_e(T,T_0',\varepsilon_{\perp})$ corresponding to $\gamma' = \gamma/2 = 2.4$ and $A' = A/10 = 0.008$ for the unilluminated and for the UV-illuminated strained material are shown as dashed lines in Figure 8b. The vertical difference between the two (dashed) curves $\Delta n_e(T,\varepsilon_{\perp}) = n_e(T,T_0,\varepsilon_{\perp}) - n_e(T,T_0',\varepsilon_{\perp})$ is again expected to describe the refractive index modulation between the dark and the UV-illuminated regions of the strained sample. Consequently, it follows that at room temperature, the refractive index modulation and consequently also the diffraction efficiency in the strained sample should be larger than in the unstrained sample, while at T = 75 °C, it should be vice versa.

However, the experimental results on the influence of $\varepsilon_{\perp}$ (and of the corresponding stress $\sigma_{\perp}$) on the diffraction efficiency of the grating structures are quite different from the predictions described above. We attribute this discrepancy to the formation of shear–stripe domains [34,41,42], which is not at all included in the presented model. The domain structure causes an additional refractive index modulation that competes with the modulation induced by the holographic patterning. The shear–stripe domains are always oriented along the straining direction. The experimental results

shown in Figure 5 suggest that when those domains are oriented perpendicular to the line patterning from the holographic structure, they cause a reduction of the diffraction efficiency from the holographic pattern. In contrast, when they are oriented parallel to the line patterning from the holographic structure, both modulations constructively support each other, and consequently, the diffraction efficiency is considerably increased.

The width of the stripe domains increases with the increasing temperature and in the vicinity of T_0, the sample area probed by the probe beam is more or less in a single domain state [34]. Consequently, the influence of domains on the diffraction efficiency is expected to decrease by the increasing temperature. This is in agreement with the results shown in Figures 6 and 7, which reveal that at $T = 75$ °C, the diffraction effects observed for $\varepsilon_{\perp}$ and $\varepsilon_{\parallel}$ are quite similar.

5. Conclusions

Our results demonstrate that macroscopically aligned LS-LCEs are very convenient materials for the fabrication of mechanically stretchable optical diffractive structures. For the investigated straining in the range of $0 < \varepsilon < 0.15$, the characteristic periodicity of the diffraction patterns changes proportionally to ε in a reversible manner. At room temperature, straining in the direction along the initial alignment direction is accompanied only with a relatively weak decrease of the diffraction efficiency, which, if necessary, can be compensated by a suitable increase of the optical power of the incident beam. Consequently, LS-LCEs are very promising for application in mechanically tunable optical devices that require predominantly a unidirectional tunability, such as for instance tunable diffraction gratings or optical filters. In devices that require straining in various directions, such as zone-plate lenses, the appearance of shear–stripe domains might bring some inconvenient effects on the diffractive properties. To be able to avoid those effects, further investigations are needed to attain better understanding on the interconnection between the stripe domain structure and the extrinsically imposed refractive index modulation.

Author Contributions: V.D. fabricated the samples, M.G. and L.H. performed measurements, M.Č. and D.B. performed theoretical analysis and I.D.-O. was cordinting the research and writing the manuscript.

Funding: This research was funded by the Slovenian Research Agency (ARRS) within the research program P1-0192.

Conflicts of Interest: The authors declare that there are no conflicts of interest.

References

1. Warner, M.; Terentjev, E.M. *Liquid Crystal Elastomers*, revised ed.; Oxford University Press: New York, NY, USA, 2007; p. 424. ISBN 9780198527671.
2. Finkelmann, H.; Nishikawa, E.; Pereira, G.G.; Warner, M. A new opto-mechanical effect in solids. *Phys. Rev. Lett.* **2001**, *87*, 015501. [CrossRef] [PubMed]
3. Corbett, D.; Warner, M. Changing liquid crystal elastomer ordering with light-a route to opto-mechanically responsive materials. *Liq. Cryst.* **2009**, *36*, 1263–1280. [CrossRef]
4. Sungur, E.; Li, M.H.; Taupier, G.; Boeglin, A.; Romeo, M.; Mery, S.; Keller, P.; Dorkenoo, K.D. External stimulus driven variable-step grating in a nematic elastomer. *Opt. Express* **2007**, *15*, 6784–6789. [CrossRef] [PubMed]
5. Zhao, Y.; Ikeda, T. *Smart Light Responsive Materials–Azobenzene-Containing Polymers and Liquid Crystals*; Wiley-Interscience: Hoboken, NJ, USA, 2009; p. 363. ISBN 9780470175781.
6. Domenici, V.; Ambrožič, G.; Čopič, M.; Lebar, A.; Drevenšek-Olenik, I.; Umek, P.; Zalar, B.; Zupančič, B.; Žigon, M. Interplay between nematic ordering and thermomechanical response in a side-chain liquid single crystal elastomer containing pendant azomesogen units. *Polymer* **2009**, *50*, 4837–4844. [CrossRef]
7. Devetak, M.; Zupancič, B.; Lebar, A.; Umek, P.; Zalar, B.; Domenici, V.; Ambrožič, G.; Žigon, M.; Čopič, M.; Drevenšek-Olenik, I. Micropatterning of light-sensitive liquid-crystal elastomers. *Phys. Rev. E* **2009**, *80*, 050701. [CrossRef] [PubMed]

8. Gregorc, M.; Zalar, B.; Domenici, V.; Ambrozič, G.; Drevenšek-Olenik, I.; Fally, M.; Čopič, M. Depth profile of optically recorded patterns in light-sensitive liquid-crystal elastomers. *Phys. Rev. E* **2011**, *84*, 031707. [CrossRef] [PubMed]
9. Tašič, B.; Li, W.; Sanchez-Ferrer, A.; Čopič, M.; Drevenšek-Olenik, I. Light-induced refractive index modulation in photoactive liquid-crystalline elastomers. *Macromol. Chem. Phys.* **2013**, *214*, 2744–2751. [CrossRef]
10. Gregorc, M.; Li, H.; Domenici, V.; Ambrožič, G.; Čopič, M.; Drevenšek-Olenik, I. Optical properties of light-sensitive liquid-crystal elastomers in the vicinity of the nematic-paranematic phase transition. *Phys. Rev. E* **2013**, *87*, 022507. [CrossRef] [PubMed]
11. Prijatelj, M.; Ellabban, M.A.; Fally, M.; Domenici, V.; Čopič, M.; Drevenšek-Olenik, I. Peculiar behaviour of optical polarization gratings in light-sensitive liquid crystalline elastomers. *Opt. Mater. Express* **2016**, *6*, 961–970. [CrossRef]
12. Gregorc, M.; Li, H.; Domenici, V.; Drevenšek-Olenik, I. Tunable photonic structures from liquid crystal elastomers. *Proc. SPIE* **2012**, *8556*, 855616.
13. White, T.J.; De Broer, D.J. Programmable and adaptive mechanics with liquid crystal polymer networks and elastomers. *Nat. Mater.* **2015**, *14*, 1087–1098. [CrossRef] [PubMed]
14. Lebar, A.; Kutnjak, Z.; Žumer, S.; Finkelmann, H.; Sánchez-Ferrer, A.; Zalar, B. Evidence of supercritical behavior in liquid single crystal elastomers. *Phys. Rev. Lett.* **2005**, *94*, 197801. [CrossRef] [PubMed]
15. Cordoyiannis, G.; Lebar, A.; Zalar, B.; Žumer, S.; Finkelmann, H.; Kutnjak, Z. Criticality controlled by cross-linking density in liquid single-crystal elastomers. *Phys. Rev. Lett.* **2007**, *99*, 197801. [CrossRef] [PubMed]
16. Petelin, A.; Čopič, M. Strain dependence of the nematic fluctuation relaxation in liquid-crystal elastomers. *Phys. Rev. E* **2010**, *82*, 011703. [CrossRef] [PubMed]
17. Cmok, L.; Petelin, A.; Čopič, M. Nematic fluctuations and semisoft elasticity in swollen liquid-crystal elastomers. *Phys. Rev. E* **2015**, *91*, 042502. [CrossRef] [PubMed]
18. Hogan, P.M.; Tajbakhsh, A.R.; Terentjev, E.M. UV manipulation of order and macroscopic shape in nematic elastomers. *Phys. Rev. E* **2002**, *65*, 041720. [CrossRef] [PubMed]
19. Sánchez-Ferrer, A. Light-induced disorder in liquid-crystalline elastomers for actuation. *Proc. SPIE* **2011**, *8107*, 810702.
20. Sánchez-Ferrer, A.; Merekalov, A.; Finkelmann, H. Opto-mechanical effect in photoactive nematic side-chain liquid-crystalline elastomers. *Macromol. Rapid Commun.* **2011**, *32*, 671–678. [CrossRef] [PubMed]
21. Ware, T.H.; Biggins, J.S.; Shick, A.F.; Warner, M.; White, T.J. Localised soft elasticity in liquid crystal elastomers. *Nat. Commun.* **2016**, *7*, 10781. [CrossRef] [PubMed]
22. Garcia-Amorós, J.; Martínez, M.; Finkelmann, H.; Velasco, D. Photoactuation and thermal isomerisation mechanism of cyanoazobenzene-based liquid crystal elastomers. *Phys. Chem. Chem. Phys.* **2014**, *16*, 8448–8454. [CrossRef] [PubMed]
23. Ware, T.H.; White, T.J. Programmed liquid crystal elastomers with tunable actuation strain. *Polym. Chem.* **2015**, *6*, 4835–4844. [CrossRef]
24. Kupfer, J.; Finkelmann, H. Nematic liquid single crystal elastomers. *Makromol. Chem. Rapid Commun.* **1991**, *12*, 717–726. [CrossRef]
25. Milavec, J.; Devetak, M.; Li, J.; Rupp, R.A.; Yao, B.; Drevenšek-Olenik, I. Effect of structural modifications on the switching voltage of a holographic polymer-dispersed liquid crystal lattice. *J. Opt.* **2010**, *12*, 015106. [CrossRef]
26. Fally, M.; Ellabban, M.; Drevenšek-Olenik, I. Out-of-phase mixed holographic gratings: A quantative analysis. *Opt. Express* **2008**, *16*, 6528–6536. [CrossRef] [PubMed]
27. Sabel, T.; Lansen, M.C. Volume holography: Novel matherials, methods and applications. In *Holographic Matherials and Optical Systems*; Naydenova, I., Babeva, T., Nazarova, D., Eds.; IntechOpen: London, UK, 2017; ISBN 978-953-51-3038-3. [CrossRef]
28. Kumar, G.S.; Neckers, D.C. Photochemistry of azobenzene-containing polymers. *Chem. Rev.* **1989**, *89*, 1915–1925. [CrossRef]
29. Sobolewska, A.; Miniewicz, A.; Grabiec, E.; Sek, S. Holographic grating recording in azobenzene functionalized polymers. *Cent. Eur. J. Chem.* **2006**, *4*, 266–284. [CrossRef]

30. Gregorc, M.; Li, H.; Domenici, V.; Ambrožič, G.; Čopič, M.; Drevenšek-Olenik, I. Kinetics of holographic recording and spontaneous erasure processes in light-sensitive liquid crystal elastomers. *Materials* **2012**, *5*, 741–753. [CrossRef] [PubMed]
31. Tóth-Katona, T.; Cigl, M.; Fodor-Csorba, K.; Hamplová, V.; Jánossy, I.; Kašpar, M.; Vojtylová, T.; Hampl, F.; Bubnov, A. Functional photochromic methylhydrosiloxane-based side-chain liquid-crystalline polymers. *Macromol. Chem. Phys.* **2014**, *215*, 742–752. [CrossRef]
32. Ryabchun, A.; Wegener, M.; Gritsai, Y.; Sakhno, O. Novel effective approach for the fabrication of PDMS Based elastic volume gratings. *Adv. Opt. Mater.* **2016**, *4*, 169–176. [CrossRef]
33. Verwey, G.; Warner, M.; Terentjev, E.M. Elastic instability and striped domains in liquid crystalline elastomers. *J. Phys.* **1996**, *6*, 1273–1290.
34. De Luca, M.; DeSimone, A.; Petelin, A.; Čopič, M. Sub-stripe pattern formation in liquid crystal elastomers: Experimental observations and numerical simulations. *J. Mech. Phys. Solids* **2013**, *61*, 2161–2177. [CrossRef]
35. De Sio, L.; Caputo, R.; De Luca, A.; Veltri, A.; Umeton, C.; Sukhov, A.V. In situ optical control and stabilization of the curing process of holographic gratings with a nematic film–polymer-slice sequence structure. *Appl. Opt.* **2006**, *45*, 3721–3727. [CrossRef] [PubMed]
36. De Jeu, W.H. *Liquid Crystal Elastomers: Materials and Applications*, 1st ed.; Springer: Berlin, Germany, 2012; p. 244. ISBN 9783642315817.
37. Yusuf, Y.; Minami, N.; Yamaguchi, S.; Cho, D.-U.; Cladis, P.E.; Brand, H.R.; Finkelmann, H.; Kai, S. Shape anisotropy and optical birefringence measurements of dry and swollen liquid sigle crystal elastomers. *J. Phys. Soc. Jpn.* **2007**, *76*, 073602. [CrossRef]
38. Greve, A.; Finkelmann, H. Nematic elastomers: The dependence of phase transformation and orientation processes on crosslinking topology. *Macromol. Chem. Phys.* **2001**, *202*, 2926–2946. [CrossRef]
39. Finkelmann, H.; Greve, A.; Warner, M. The elastic anisotropy of nematic elastomers. *Eur. J. Phys. E* **2001**, *5*, 281–293. [CrossRef]
40. Lazo, I.; Neal, J.; Palffy-Muhoray, P. Determination of the Refractive Indices of Liquid Crystal Elastomers. 2008. Available online: http://nlcmf.lci.kent.edu/reference_materials/student_research/israel_lazo_refractive_indexpdf.pdf (accessed on 28 June 2018).
41. Zubarev, E.; Kuptsov, S.A.; Yuranova, T.I.; Talroze, R.V.; Finkelmann, H. Monodomain liquid crystalline networks: Reorientation mechanism from uniform to stripe domains. *Liq. Cryst.* **1999**, *26*, 1531–1540. [CrossRef]
42. Urayama, K.; Mashita, R.; Kobayashi, I.; Takigawa, T. Stretching-induced director rotation in thin films of liquid crystal elastomers with homeotropic alignment. *Macromolecules* **2007**, *40*, 7665–7670. [CrossRef]